NIH Public Access
Author Manuscript
Microsc Microanal. Author manuscript; available in PMC 2012 January 22.

Published in final edited form as:
Microsc Microanal. 2011 October ; 17(5): 779–787. doi:10.1017/S1431927611011925.

Quantification of Collagen Organization and Extracellular Matrix Factors within the Healing Ligament

Connie S. Chamberlain[1], **Erin M. Crowley**[1], **Hirohito Kobayashi**[1], **Kevin W. Eliceiri**[2,3], and **Ray. Vanderby**[1,3]

[1]Department of Orthopedics and Rehabilitation, University of Wisconsin, Madison, WI, USA

[2]Laboratory for Optical and Computational Instrumentation, University of Wisconsin, Madison WI, USA

[3]Department of Biomedical Engineering, University of Wisconsin, Madison, Wisconsin 53705 USA

Abstract

Ligament healing of a grade III injury (i.e. a complete tear) involves a multifaceted chain of events that forms a neoligament, which is more scar-like in character than the native tissue. The remodeling process may last months or even years with the injured ligament never fully recovering pre-injury mechanical properties. With tissue engineering and regenerative medicine, understanding the normal healing process in ligament and quantifying it provide a basis to create and assess innovative treatments. Ligament fibroblasts produce a number of ECM components, including collagen types I and III, decorin and fibromodulin. Using a combination of advanced histology, molecular biology and nonlinear optical imaging approaches, the early ECM events during ligament healing have been better characterized and defined. First, the dynamic changes in ECM factors after injury are shown. Second, the factors associated with creeping substitution are identified. Finally, a method to quantify collagen organization is developed and used. Each ECM factor described herein as well as the temporal quantification of fiber organization helps elucidate the complexity of ligament healing.

Introduction

Ligament healing of a grade III injury (i.e. a complete tear) involves a multifaceted chain of events that forms a neoligament, which is more scar-like in character than the native tissue. The remodeling process may last months or even years with the injured ligament never fully recovering pre-injury mechanical properties (Levenson et al. 1965, Lin et al. 2004). In an effort to improve upon this suboptimal process, researchers have tested a number of treatments including tissue engineering approaches, nonsteroidal anti-inflammatory drugs, ultrasonic and electrical stimulation (Lin et al. 2004, Marsolais et al. 2001). However, an incomplete understanding of the healing process makes development of an optimal treatment difficult. With tissue engineering and regenerative medicine, understanding the normal healing process in ligament and quantifying it provide a basis to create and assess innovative treatments.

The nonlinear optical microscopy technique of Multiphoton Laser Scanning Microscopy (MPLSM) (Denk et al. 1990) provides high-resolution imaging of endogenous (Provenzano

Address for reprint requests and other correspondence: R. Vanderby, Dept. of Orthopedics and Rehabilitation, Orthopedic Research Laboratories, 1111 Highland Ave., WIMR Room 5059, University of Wisconsin, Madison, WI 53705; (Telephone: (608)-263-9593; Fax (608)-265-6450; vanderby@ortho.wisc.edu).

NIH-PA Author Manuscript
NIH-PA Author Manuscript
NIH-PA Author Manuscript

NIH-PA Author Manuscript

NIH-PA Author Manuscript

NIH-PA Author Manuscript

et al. 2008) and exogenous fluorescent proteins (White et al. 2001), all with good viability and improved imaging depth (Centonze, White 1998, Squirrell et al. 1999) compared to other light microscopy methods. While much of the MPLSM work has been for in vitro and in vivo cellular applications, recent studies reveal MPLSM's potential for imaging histopathology slides by revealing additional information in the H&E staining not seen by traditional light microscopy (Masters 2009).

Previously, this lab used histology and microangiography to examine early ligament healing in a grade III injury model (Chamberlain et al. 2009). Our results illustrate that transection of the medial collateral ligament (MCL) initiates a response where inflammatory cells, mitotic cells, apoptotic cells and angiogenic factors are significantly increased throughout the first four weeks of healing. During this time a creeping substitution occurs where granulation tissue progressively infiltrates and disrupts the adjacent uninjured matrix, resulting in ECM degradation beyond the original site of injury (Chamberlain et al. 2009). Although our previous study recognized a number of cellular factors associated with ligament healing and matrix degradation, the specific matrix components have not been identified.

Ligament fibroblasts produce a number of ECM components, including collagen types I and III, decorin and fibromodulin. Type I collagen comprises 95% of the total ligamentous collagen, but smaller amounts of types III, V, XII, and XIV collagen are also present (Nordin M., Lorenz T., Campello M 2001). The fibrillar type III collagen forms heterogeneous collagen fibrils with type I collagen but may inhibit collagen fibril diameter growth. Surrounding the collagen fibrils is a ground substance consisting of proteoglycans and glycosaminoglycans (Nordin M., Lorenz T., Campello M 2001). Two abundant proteoglycans within the ligament include decorin and fibromodulin. These proteoglycans bind type I collagen and regulate collagen fibrillogenesis. Collectively, collagen confers remarkable strength to the ligament and the proteoglycans maintain tissue hydration and affect fibril maturation. However, the localization and association of collagen with the proteoglycans during wound healing remains largely unknown. Provenzano (Provenzano et al. 2005) demonstrated an increase in mRNA of collagen types I and III, decorin and fibromodulin at 7 days after a grade II sub-failure (sprain) ligament injury. This injury healed with minimal inflammation and the ligamentous tissue appeared to regenerate, albeit over a longer time span. The increase of these ECM factors after a grade II injury allows us to hypothesize that ECM factors are altered differently after a grade III injury where inflammation and scar tissue are induced. Additionally, myofibroblasts increase within the wound site after a grade III rupture. Myofibroblasts are transdifferentiated fibroblasts that promote wound contraction but persist during excessive scarring (Desmouliere et al. 2005). Herein, we study the spatial and temporal localization of procollagen type I, collagen type III, fibromodulin, decorin, and myofibroblasts via immunohistochemistry during healing and early scar formation. Additionally, we quantify collagen organization at various early time points in the healing process using multiphoton microscopy.

Materials and Methods

Animals

This study was approved by the University of Wisconsin Institutional Animal Use and Care Committee. Thirty skeletally mature Wistar rats were used as an animal model for ligament healing. Each group was randomly placed in 1 of 10 groups (n=3/group; 1, 3, 5, 7, 9, 11, 14, 21, or 28 days, control). Rats were anesthetized via isofluorane. A surgically transected, rather than torn, medial collateral ligament (MCL) was used as an experimental model to create a uniform defect for healing. Each rat was subjected to bilateral MCL transections using sterile techniques. A small, 1cm skin incision was made over the medial aspect of each

NIH-PA Author Manuscript

NIH-PA Author Manuscript

NIH-PA Author Manuscript

stifle and the subcutaneous tissue was dissected to expose the sartorius muscle and underlying MCL. The mid-point of the MCL (determined using a scaled scalpel handle) was completely transected. Severed ends were not sutured and allowed to retract. The muscular, subcutaneous and subdermal tissue layers were each closed with 4-0 Dexon suture. Another group of 3 animals underwent no transection and served as intact controls. All animals were allowed unrestricted cage movement immediately after surgery. At days 1, 3, 5, 7, 9, 11, 14, 21 or 28 post-surgery the animals were sacrificed. The MCLs were carefully dissected, measured, weighed, and immediately placed in Optimal Cutting Temperature (OCT) for flash freezing. Longitudinal cryosections were then cut at a 5 μm thickness, mounted on Superfrost plus microscope slides and maintained at −70º C. Each section was subjected to H&E staining and multiphoton microscopy or to immunohistochemistry.

Multiphoton Microscopy

MPLSM was performed on all samples previously subjected to H&E staining. Samples were imaged using an optical workstation that was assembled around a Nikon Eclipse TE300. A Ti:sapphire laser (890 nm; Spectra-Physics-Millennium/Tsunami, Mountain View, CA) was utilized to generate multiphoton excitation (Wokosin et al. 2003). The laser was focused onto the sample using a Nikon 60X Plan Apo oil-immersion lens (for manuscript images; numerical aperture =1.4) or a Nikon 40X SuperFluor (for quantification purposes; numerical aperture=1.3). Second harmonic generation (SHG) filters were not utilized systematically since while unfixed and unstained ligament did have SHG signal on this system (data not shown) it was far less than the H&E slides. This can be explained in two ways. First, is that the MPLSM utilized only detects backwards SHG and not in the forwards direction, so some signal is lost. Second, the signal of collagen is enhanced by the eosin which fluorescences very well at the wavelength of 890nm. The eosin from the H&E stain provided ample fluorescence to capture and elucidate the organizational process of collagen fibers during ligament healing (data not shown). Images were captured using WiscScan, a software package developed at LOCI (Laboratory for Optical and Computational Instrumentation, University of Wisconsin, Madison, WI). Corresponding H&E images were captured to validate the MPLSM images. Collagen organization within the transected region (region of interest; ROI) was quantified by the tissue elliptical axis ratio (TEAR) parameter originally used to characterize an Achilles' tendon ultrasound image for diagnostic purposes (Tuthill et al. 1999, Bashford et al. 2008). Three images per animal per time point were obtained randomly within the healing region. The 2-D spatial frequency spectrum was evaluated for the ROI in each image, applying 2 dimensional fast Fourier transformation (2D FFT). The TEAR of the image corresponded to the ratio of major radius-to–minor radius of ellipse and measured the degree of collagen orientation. A TEAR=1 indicates zero organization, i.e. a completely random set of fiber directions. The higher the TEAR metric, the more the fibers are preferentially oriented along the axis of the ligament.

Immunohistochemistry

Immunohistochemical (IHC) analysis was performed on frozen sections using mouse monoclonal or rabbit polyclonal antibodies. Sections were fixed with acetone and exposed to 3% hydrogen peroxide to eliminate endogenous peroxidase activity. To verify that chondroitin sulfate chains in the proteoglycan core did not interfere with decorin or fibromodulin antibody binding, representative samples were treated with 1.25 U/ml of chondroitinase from Proteaus vlugaris (Sigma-Aldrich, St. Louis, MO) for 10 minutes at 37º C. A blocking step using Background Buster (Innovex Biosciences, Richmond, CA) was applied after hydrogen peroxide application before being incubated with rabbit or mouse primary antibody. Sections were then incubated with biotin and strepavidin-conjugated to horseradish peroxidaseusing the Stat Q staining kit (Innovex Biosciences, Richmond, CA). The bound antibody complex was visualized using diaminobenzidine (DAB). Stained

NIH-PA Author Manuscript

NIH-PA Author Manuscript

NIH-PA Author Manuscript

sections were dehydrated, cleared, cover-slipped and viewed under light microscopy. Negative controls omitting the primary antibody were included with each experiment. Positive controls of gut or spleen were also included. Mouse or rabbit monoclonal antibodies to type I procollagen (Developmental Hybridoma, Iowa City, IA), α-smooth muscle actin (Biogenex, San Roman, CA), type III collagen (Sigma-Aldrich,St. Louis, MO), fibromodulin (Santa Cruz, Santa Cruz, CA), and decorin (Sigma-Aldrich, St. Louis, MO) were utilized. After IHC, α-smooth muscle actin was counterstained with hematoxylin.

Cell counting

After IHC/IF staining, micrographs were collected using a camera assisted microscope (Nikon Eclipse microscope, model E6000 with an Olympus camera, model DP79). Six blocked random pictures were obtained from each sample at an original magnification of 400X. Images were captured randomly within the healing region (HR), distal (dHR) and proximal (pHR) edges of the healing region, epiligament (EL), and distal (distal) and proximal (prox) ends of the MCL (Fig.1). One section was counted per animal resulting in 3 sections per time point. The intensity of each immunohistochemical marker within the captured image was then quantified with Image J (National Institutes of Health).

Statistical Methods

For all immunohistochemical analyses, a two-way ANOVA was first used to assess differences between groups (day, normal), and regions (HR, pHR, dHR, prox, distal, and EL), with region nested within animal; the interaction term was not included. Then a one-way ANOVA on region was fitted to assess differences adjusted for day/group. Finally, a one-way ANOVA was used to test for differences across groups within each region. Diagnostic plots of residuals were examined for gross violations of the assumptions of ANOVA, and if so, transformations of the dependent variable were considered. All factors required a logarithmic transformation ($y = \ln(x + 0.1)$) in order to satisfy the assumptions of ANOVA. MPLSM data are presented as the least squares means ± SE of measurements for triplicate sections from each animal. A one-way ANOVA was used to assess differences between groups (day, cx). For all experiments, if the overall p-value for the F-test in ANOVA was significant, pair-wise comparisons were obtained (Fisher's LSD). All P-values reported are two sided. The criterion for statistical significance was $p < 0.05$. All computations and figures were done in R for Windows, version 2.5.1 patched (2007-07-10 r42164; (R Development Core Team 2006) and/or Microsoft Office Excel (XLSTAT 2009.4.05).

Results

Multiphoton microscopy

MPLSM analysis of the H&E-stained ligament allowed for the clear visualization of collagen morphology. The uninjured ligament demonstrates aligned collagen fibers with few cells (Fig. 2A). The corresponding H&E images (Fig. 2B) confirm the hypocellularity and organization of the normal ligament that was captured by MPLSM. One day post-injury the transected region is clearly discernible via dense collagenous tissue abutting the less collagenous, more porous, provisional matrix (Fig. 2C-D). Formation of granulation tissue at day 3 results in fewer gaps within the healing region compared to day 1 whereas the uninjured region is similarly dense and discernible (Fig. 2E-F). By day 5 the collagen that borders the healing region integrates into the granulation tissue (Fig. 2G-H). The granulation tissue continues to incorporate the uninjured ligament portion from days 7-11 (Fig. 2I-N). Collagen fibers are also more apparent due to the sparse and irregular organization (Fig. 2I-N). As the ligament undergoes remodeling from days 14-28, the intensity of collagen by

NIH-PA Author Manuscript

NIH-PA Author Manuscript

NIH-PA Author Manuscript

MPLSM is stronger as collagen becomes denser and more organized while individual collagen fibrils are less obvious (Fig. 2O-T).

Measurement of collagen organization by TEAR verifies the increasing disorganization during the first week of healing (Fig. 3). Uninjured ligament results in an average TEAR of 5.33 (SEM ± 0.56). The more disorganized collagen becomes, the lower the TEAR. Collagen disorganization is significantly different from the intact control from days 1-21 ($p < .05$). Organization steadily improves across time as demonstrated via H&E and MPLSM images, but clear deformities exist when compared to the intact control. Alignment improves by day 28 (4.44 ± 0.65) and is somewhat comparable to the intact control ($p = .056$). However, collagen alignment flaws remain and tissue remains hypercellular (Fig. 2S-T), likely contributing to the mechanical inferiority exhibited by the injured ligament (Levenson et al. 1965, Lin et al. 2004).

Immunohistochemistry

Immunohistochemistry of damaged ligaments localizes the injury response of ECM proteins within the tissue (Figs. 4 and 5A-B). Type I procollagen disperses throughout the uninjured MCL (Fig.5). After injury, levels remain similar to the intact control until day 7 (Fig. 5A-B). Type I procollagen then significantly decreases at day 7 and remains low until day 28, excluding an intermediate rise at day 14. The spatial distribution of type I procollagen further clarifies the aforementioned temporal results (Fig. 4). Type I procollagen localizes throughout the intact ligament (Fig. 4A), but injury alters its spatial distribution. The provisional matrix contains little type I procollagen at day 1 (Fig. 4E). The distal and proximal HR edges decrease in type I collagen content at day 5 as additional ECM becomes disorganized during granulation tissue formation (Fig. 4I). However, type I procollagen production is evident within the granulation tissue, although the amount is not equal to that of the intact ligament (Fig. 4M).

The production of procollagen type I and collagen type III differs substantially from one another after injury (Fig. 5A-B). A paucity of type III collagen localizes to the intact MCL except the epiligament (Fig. 4B). One day after injury, total type III collagen production is similar to the intact control, but increases within the provisional matrix of the healing region (Fig. 4F). Concomitant with granulation tissue formation on day 3, type III collagen significantly infiltrates the healing region and its edges, creeps through the ligament on day 5-7 (Figs. 4J and 4N) and remains high until day 28. Essentially the entire ligament contains type III collagen by the end of the study.

Decorin production follows a pattern similar to type I procollagen (Fig. 5A-B). Decorin is prevalent throughout the control ligament as well as in the uninjured portion of the early healing MCL and the epiligament (Figs. 4C and 4G). Some decorin is produced in the provisional matrix one day after injury (Fig. 4G), but overall production does not significantly differ from the intact ligament until day 5 (Fig. 5). The limited decorin within the granulation tissue clearly discerns the borders to the decorin-positive uninjured portion (Fig. 4K). As the granulation tissue expands throughout the tissue and procollagen continues to decrease, decorin levels also diminish (Fig. 4O). Overall levels remain low until day 28.

Fibromodulin localization differs substantially from decorin and type I procollagen (Fig. 5A-B). In contrast to decorin, less fibromodulin localizes to the intact MCL than the injured ligament (Fig. 4D). Moreover, very little fibromodulin localizes to the epiligament. Injury stimulates the production of fibromodulin from day 1 to day 28. Spatially, fibromodulin significantly increases within the day 1 provisional matrix (Fig. 4H) and remains constant within the granulation tissue (Figs. 4L and 4P) until day 28.

NIH-PA Author Manuscript

NIH-PA Author Manuscript

NIH-PA Author Manuscript

Smooth muscle actin results are presented in figure 6. This marker stains for both differentiated myofibroblasts and smooth muscle cells. The concentration of α-SMA is low within the control ligament as well as the early healing MCL. A significant increase of α-SMA above the control occurs 5 days post-injury and appears to localize primarily within the blood vessels (Fig. 6 left inset). As granulation tissue incorporates into the ligament, α-SMA identifying myofibroblasts (Fig. 6 middle inset) crests between day 7 and 14 and remains above control levels up to day 28. Spatially, α-SMA significantly appears at the HR edges between days 5 and 7, but both regions return to control levels by day 28. The epiligament contains the highest concentration of blood-vessel related-α-SMA throughout healing and is steadily maintained (Fig.6 right inset).

Discussion

Results in this study help define the early ECM events during ligament healing. First, the dynamic changes in ECM factors after injury are shown. Second, the factors associated with creeping substitution are identified. Finally, a method to quantify collagen organization is developed and used. Each ECM factor described herein as well as the temporal quantification of fiber organization helps elucidate the complexity of ligament healing.

As previously reported for ligament healing, granulation tissue initially forms at the injury, but then expands via creeping substitution into the adjacent tissues (Chamberlain et al. 2009). Creeping substitution appears as a catabolic process involved in tissue remodeling. Type I procollagen and decorin primarily localize outside the creeping substitution borders resulting in reduced amounts overall as creeping substitution progresses. In contrast, type III collagen localizes to both intact and granulation tissue and increases with injury. As a result, type I collagen, the most prevalent protein in ligament decreases and is replaced by the scar-forming type III collagen as granulation tissue expands and remodeling progresses. This data further validates the association of creeping substitution and scar formation.

To our knowledge, the significant reduction of decorin within the developing granulation tissue and the increase in fibromodulin of the healing ligament is a new finding. Decorin and fibromodulin bind to collagen type I and II at different sites of the molecules to modulate fibrillogenesis (Hedbom, Heinegard 1989, Scott 1988, Brown, Vogel 1989). Prior knockout studies demonstrate the different functional roles of the small leucine-rich repeat proteoglycans (SLRPs) during fibrillogenesis (Danielson et al. 1997, Matheson et al. 2005). The targeted disruption of decorin results in abnormally large collagen fibrils, and fragility of skin (Danielson et al. 1997), whereas the disruption of fibromodulin increases thinning of ligament bundles (Matheson et al. 2005) and reduces tendon stiffness. Besides its role in fibril maturation and tissue hydration, decorin functions to maintain the ECM in a quiescent state by down-regulating cell migration, proliferation and protein synthesis (Iozzo 1999) and therefore producing an anti-fibrotic effect (Gray et al. 1999). With ligament injury decorin is reduced in the healing tissue while cellular factors and ECM protein synthesis are concurrently up-regulated. The down-regulation of decorin is likely to alter normal fibrillogenesis and inhibit the regeneration of normal tissue. Strong localization of decorin to the intact portion of the ligament rather than the injured region affirms the inhibition of decorin within the hypercellular granulation tissue.

Unlike decorin, fibromodulin stimulates formation of mature large collagen fibrils (Jepsen et al. 2002). Similar to levels of type III collagen, fibromodulin increases immediately following injury and remains elevated throughout the 4 weeks studied here. These results are similar to those of the inflamed periodontal ligament (Qian et al. 2004). Fibromodulin is widely distributed within the healthy periodontal connective tissues, but an inflammatory response further enhances fibromodulin within the compromised tissue (Qian et al. 2004).

NIH-PA Author Manuscript

NIH-PA Author Manuscript

NIH-PA Author Manuscript

Fibromodulin is likewise detected in granulation tissue of a pulmonary fibrotic model (Venkatesan et al. 2000). The current results agree with studies in other injured tissues showing the up-regulation of fibromodulin during healing.

Following injury, fibroblasts activate and migrate into damaged tissue and differentiate into contractile and secretory myofibroblasts, contributing to tissue repair. Currently no marker exists to label fibroblasts whereas α-smooth muscle actin identifies differentiated myofibroblasts and smooth muscle cells. Most α-SMA localizes within the granulation tissue, but does not follow the typical creeping substitution pattern. Initially, α-SMA localizes first to the edges of the healing region and then, concomitantly, to the original transected region and ligament ends. This atypical patterning is likely accounted for by the up regulation of both the newly formed blood vessels at the healing region edges (i.e. granulation tissue border) and the myofibroblasts within the original transected region of the granulation tissue.

Published studies (typically with fewer time points) support the early healing events of the MCL reported here. Thus, this study seems to be a reasonable model of soft-tissue-to-soft-tissue healing in an extra-capsular ligament. Clearly, healing differences may arise with joint immobilization, segmental defects, subfailure damage, different ligaments, or other perturbations in healing ligament models. For example, joint immobilization of the MCL has not demonstrated any significant advantages to healing (Thornton et al. 2005), whereas immobilization after ACL reconstruction improves bone-tendon integration and reduces the inflammatory response (Dagher et al. 2009). Subfailure ligament healing (i.e. grade II sprains) (Provenzano et al. 2005) demonstrates an increase in decorin, fibromodulin, and collagen types I and III mRNA at 7 days post-sprain. Type I collagen expression is also significantly greater than type III collagen expression of a grade II injury. This behavior resulted in more regenerative healing than what is observed in the current study. The current grade III injury only shows increases in fibromodulin and type III collagen. Moreover, type III collagen is 53% greater than type I procollagen in a grade III injury at day 7. This discrepancy is not surprising because a grade II injury does not stimulate an inflammatory reaction and subsequent cell migration and proliferation which are required for controlling extracellular matrix scar formation. In contrast, a grade III injury initiates a considerable inflammatory response, mitotic reaction, and extensive collagen reorganization due to the dramatic infiltration of fibroblasts and formation of granulation tissue. These spatiotemporal data show a detailed cascade of events in the early healing of an extra-capsular ligament.

In an effort to understand and define the dynamic changes of the ECM in the healing ligament, multiphoton microscopy was included in this study. To our knowledge, this is the first publication to describe, compare, and quantify the temporal aspects of collagen organization using 2D FFT on H&E-stained, MPLSM-captured, healing ligament tissue. MPLSM allows for high resolution non-invasive imaging of physiology, morphology and cell-cell interactions in tissue sections, intact tissues, and live animals. Collagen is a significant light dispersing component. Transection and subsequent healing of a ligament perturbs the normal collagen content and organization and hence, the scattering properties of the tissue are also perturbed. This portion of the study demonstrates collagen organization more clearly than standard H&E analysis. In conjunction with 2D FFT analysis, MPLSM demonstrates a less collagenous, more permeable, disorganized healing. Over time, the transected region becomes less discernible as the granulation tissue incorporates into the surrounding intact tissue. By the end of the study, the ECM becomes more organized, but matrix flaws remain. To our knowledge, this is the first report that quantifies collagen organization this way, i.e. by computing an elliptical axis ratio with 2D FFT analysis from MPLSM images. A similar quantification method on ultrasound images was used to characterize tendinopathy using an 11MHz ultrasound with a resolution of 75 μm (Bashford

NIH-PA Author Manuscript

NIH-PA Author Manuscript

NIH-PA Author Manuscript

et al. 2008). The current study utilizes a 76 MHz MPLSM, capable of obtaining optical sections with a resolution of approximately 1.1-1.5 μm. The lower resolution, ultrasound images were successfully used to quantify collagen with FFT's, suggesting its use here with the higher resolved MPLSM technique would be more accurate. The ability to clearly distinguish and quantify collagen in H&E-stained sections provides value when studying the ECM and supports the application of MPLSM imaging to analyze collagenous structures. Although unfixed and unstained ligament only provided very weak signal (attributed to backwards detected second harmonic generation signal), the eosin from the H&E stain provided ample fluorescence to capture and elucidate the organizational process of collagen fibers during ligament healing. The current experiment focused on MPLSM intensity-based imaging on unfixed H&E-stained tissue, but there are several experimental models that benefit from this technology; compared to conventional brightfield imaging approaches, MPLSM allows for improved viability, the ability to detect second harmonic generation (SHG), and the capacity to excite intrinsic fluorescence (Squirrell et al. 1999). Use of this technique may provide invaluable insight on the physiology, morphology, and cell-cell interactions in intact tissues or live animals. While confocal microscopy also provides high resolution imaging of H&E samples, MPLSM is particularly attractive for its ability to do this and simultaneously detect endogenous components. SHG has been an effective tool for studying the extracellular matrix in breast cancer. Future studies will evaluate whether SHG is similarly useful for ligament remodeling studies (i.e. the use of emerging SHG systems to detect the forwards and backwards components of SHG) (Lacomb et al. 2008). Traditionally on MPLSMs such as that used in this study, the majority of the detected MP and SHG signal is detected in the back scatter to a bottom port or side external detector. However, for future ligament studies there is great potential advantage to detect both forward and backward signals, to isolate the quasi-coherent and multiple scattered components from tissue instead of relying on the fluorescence emitted from the eosin from the H&E staining.

Disorganization of the collagenous ECM is one factor that contributes to inferior mechanical properties in healing tissues. Healing tissue must stretch further before all disorganized fibers straighten and bear load. This microstructural behavior produces a longer toe region in the stiffness curve, a lower modulus, and an uneven distribution of fiber load bearing with premature rupture of fibers that are recruited early. Other factors include altered ECM composition and concentration of collagen making a direct correlation of TEAR with mechanical properties difficult. In the first week of rat MCL healing when collagen is disorganized and its concentration is low, the ligament is almost too fragile to dissect and mechanically test. After 11 days of healing, strength is approximately 41.3-52.0% (mean: 47%) ({{1479 Provenzano,P.P. 2003, unpublished data}} of normal. This mechanical compromise corresponds to a TEAR that is 45.2% of normal ligament.

The literature shows that transected or torn ligaments do not recover completely (compositionally and morphologically), and that healing tissue is mechanically inferior. This study shows a persistent creeping of the granulation tissue that contributes to these reported problems in ligament healing. Within this granulation tissue is a collagen matrix that is initially, very disorganized (not statistically different than a random organization) and then it remodels to a more axial microstructure. However, the organization process slows and does not replicate native tissue over the time course of this study (four weeks). As collagen organization progressively improves, type I procollagen and decorin decreases while type III collagen, fibromodulin and α-smooth muscle actin increases, indicating a significantly different ligament than its original structure. In conclusion, collagen organization and the associated ECM factors can be quantified using MPLSM, fast Fourier transformation, and immunohistochemistry.

NIH-PA Author Manuscript

NIH-PA Author Manuscript

NIH-PA Author Manuscript

Acknowledgments

The authors acknowledge the contributions by Alejandro Munoz del Rio, PhD and Paolo Provenzano, PhD. Financial support was provided by the National Institutes of Health (NIH), Grant No. A536110.

References

BASHFORD GR, TOMSEN N, ARYA S, BURNFIELD JM, KULIG K. Tendinopathy discrimination by use of spatial frequency parameters in ultrasound B-mode images. IEEE Transactions on Medical Imaging. 2008; 27(5):608–615. [PubMed: 18450534]

BROWN DC, VOGEL KG. Characteristics of the in vitro interaction of a small proteoglycan (PG II) of bovine tendon with type I collagen. Matrix (Stuttgart, Germany). 1989; 9(6):468–478.

CENTONZE VE, WHITE JG. Multiphoton excitation provides optical sections from deeper within scattering specimens than confocal imaging. Biophysical journal. 1998; 75(4):2015–2024. [PubMed: 9746543]

CHAMBERLAIN CS, CROWLEY E, VANDERBY R. The spatio-temporal dynamics of ligament healing. Wound repair and regeneration : official publication of the Wound Healing Society [and] the European Tissue Repair Society. 2009; 17(2):206–215.

DAGHER E, HAYS PL, KAWAMURA S, GODIN J, DENG XH, RODEO SA. Immobilization modulates macrophage accumulation in tendon-bone healing. Clinical orthopaedics and related research. 2009; 467(1):281–287. [PubMed: 18830671]

DANIELSON KG, BARIBAULT H, HOLMES DF, GRAHAM H, KADLER KE, IOZZO RV. Targeted disruption of decorin leads to abnormal collagen fibril morphology and skin fragility. The Journal of cell biology. 1997; 136(3):729–743. [PubMed: 9024701]

DENK W, STRICKLER JH, WEBB WW. Two-photon laser scanning fluorescence microscopy. Science (New York, NY). 1990; 248(4951):73–76.

DESMOULIERE A, CHAPONNIER C, GABBIANI G. Tissue repair, contraction, and the myofibroblast. Wound repair and regeneration : official publication of the Wound Healing Society [and] the European Tissue Repair Society. 2005; 13(1):7–12.

GRAY SD, TITZE IR, CHAN R, HAMMOND TH. Vocal fold proteoglycans and their influence on biomechanics. The Laryngoscope. 1999; 109(6):845–854. [PubMed: 10369269]

HEDBOM E, HEINEGARD D. Interaction of a 59-kDa connective tissue matrix protein with collagen I and collagen II. The Journal of biological chemistry. 1989; 264(12):6898–6905. [PubMed: 2496122]

IOZZO RV. The biology of the small leucine-rich proteoglycans. Functional network of interactive proteins. The Journal of biological chemistry. 1999; 274(27):18843–18846. [PubMed: 10383378]

JEPSEN KJ, WU F, PERAGALLO JH, PAUL J, ROBERTS L, EZURA Y, OLDBERG A, BIRK DE, CHAKRAVARTI S. A syndrome of joint laxity and impaired tendon integrity in lumican- and fibromodulin-deficient mice. The Journal of biological chemistry. 2002; 277(38):35532–35540. [PubMed: 12089156]

KOLETTAS E, ROSENBERGER RF. Suppression of decorin expression and partial induction of anchorage-independent growth by the v-src oncogene in human fibroblasts. European journal of biochemistry / FEBS. 1998; 254(2):266–274. [PubMed: 9660179]

LACOMB R, NADIARNYKH O, CAMPAGNOLA PJ. Quantitative second harmonic generation imaging of the diseased state osteogenesis imperfecta: experiment and simulation. Biophysical journal. 2008; 94(11):4504–4514. [PubMed: 18281387]

LEVENSON SM, GEEVER EF, CROWLEY LV, OATES JF 3RD, BERARD CW, ROSEN H. The Healing of Rat Skin Wounds. Annals of Surgery. 1965; 161:293–308. [PubMed: 14260029]

LIN TW, CARDENAS L, SOSLOWSKY LJ. Biomechanics of tendon injury and repair. Journal of Biomechanics. 2004; 37(6):865–877. [PubMed: 15111074]

MARSOLAIS D, COTE CH, FRENETTE J. Neutrophils and macrophages accumulate sequentially following Achilles tendon injury. Journal of orthopaedic research : official publication of the Orthopaedic Research Society. 2001; 19(6):1203–1209. [PubMed: 11781025]

NIH-PA Author Manuscript

NIH-PA Author Manuscript

NIH-PA Author Manuscript

MASTERS BR. Correlation of histology and linear and nonlinear microscopy of the living human cornea. Journal of biophotonics. 2009; 2(3):127–139. [PubMed: 19343693]

MATHESON S, LARJAVA H, HAKKINEN L. Distinctive localization and function for lumican, fibromodulin and decorin to regulate collagen fibril organization in periodontal tissues. Journal of periodontal research. 2005; 40(4):312–324. [PubMed: 15966909]

MOSCATELLO DK, SANTRA M, MANN DM, MCQUILLAN DJ, WONG AJ, IOZZO RV. Decorin suppresses tumor cell growth by activating the epidermal growth factor receptor. The Journal of clinical investigation. 1998; 101(2):406–412. [PubMed: 9435313]

NASH MA, LOERCHER AE, FREEDMAN RS. In vitro growth inhibition of ovarian cancer cells by decorin: synergism of action between decorin and carboplatin. Cancer research. 1999; 59(24): 6192–6196. [PubMed: 10626812]

NORDIN, M.; LORENZ, T.; CAMPELLO, M. Basic Biomechanics of the Musculoskeletal System. Lippincott Williams and Wilkins; 2001. Biomechanics of tendons and ligament; p. 103-125.

OKSALA O, SALO T, TAMMI R, HAKKINEN L, JALKANEN M, INKI P, LARJAVA H. Expression of proteoglycans and hyaluronan during wound healing. The journal of histochemistry and cytochemistry : official journal of the Histochemistry Society. 1995; 43 (2):125–135. [PubMed: 7529785]

PROVENZANO PP, ALEJANDRO-OSORIO AL, VALHMU WB, JENSEN KT, VANDERBY R JR. Intrinsic fibroblast-mediated remodeling of damaged collagenous matrices in vivo. Matrix biology : journal of the International Society for Matrix Biology. 2005; 23(8):543–555. [PubMed: 15694131]

PROVENZANO PP, RUEDEN CT, TRIER SM, YAN L, PONIK SM, INMAN DR, KEELY PJ, ELICEIRI KW. Nonlinear optical imaging and spectral-lifetime computational analysis of endogenous and exogenous fluorophores in breast cancer. Journal of Biomedical Optics. 2008; 13(3):031220. [PubMed: 18601544]

QIAN H, XIAO Y, BARTOLD PM. Immunohistochemical localization and expression of fibromodulin in adult rat periodontium and inflamed human gingiva. Oral diseases. 2004; 10(4): 233–239. [PubMed: 15196146]

R DEVELOPMENT CORE TEAM. A language and environment for statistical computing. 2006-last updateAvailable: http://www.R-project.org

SCOTT JE. Proteoglycan-fibrillar collagen interactions. The Biochemical journal. 1988; 252(2):313–323. [PubMed: 3046606]

SQUIRRELL JM, WOKOSIN DL, WHITE JG, BAVISTER BD. Long-term two-photon fluorescence imaging of mammalian embryos without compromising viability. Nature biotechnology. 1999; 17(8):763–767.

THORNTON GM, JOHNSON JC, MASER RV, MARCHUK LL, SHRIVE NG, FRANK CB. Strength of medial structures of the knee joint are decreased by isolated injury to the medial collateral ligament and subsequent joint immobilization. Journal of orthopaedic research : official publication of the Orthopaedic Research Society. 2005; 23(5):1191–1198. [PubMed: 16140200]

TUTHILL TA, RUBIN JM, FOWLKES JB, JAMADAR DA, BUDE RO. Frequency analysis of echo texture in tendon. Ultrasound in medicine & biology. 1999; 25(6):959–968. [PubMed: 10461725]

VENKATESAN N, EBIHARA T, ROUGHLEY PJ, LUDWIG MS. Alterations in large and small proteoglycans in bleomycin-induced pulmonary fibrosis in rats. American journal of respiratory and critical care medicine. 2000; 161(6):2066–2073. [PubMed: 10852789]

WHITE JG, SQUIRRELL JM, ELICEIRI KW. Applying multiphoton imaging to the study of membrane dynamics in living cells. Traffic (Copenhagen, Denmark). 2001; 2(11):775–780.

WOKOSIN DL, SQUIRRELL JM, ELICEIRI KW, WHITE JG. Optical workstation with concurrent, independent multiphoton imaging and experimental laser microbeam capabilities. The Review of scientific instruments. 2003; 74(1):193–201. [PubMed: 18607511]

NIH-PA Author Manuscript
NIH-PA Author Manuscript
NIH-PA Author Manuscript

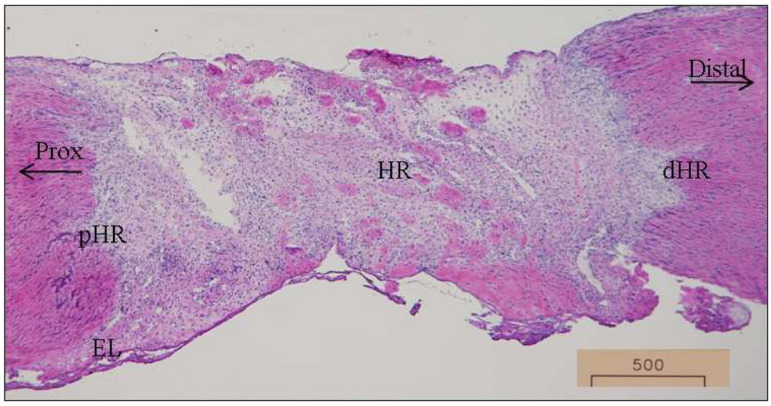

Figure 1.

Specific MCL regions analyzed for IHC .Representative day 5 micrograph to depict the specific regions within the MCL. HR: healing region; dHR: distal region of the healing region; pHR: proximal region of the healing region; distal: distal end of the MCL; prox: proximal end of the MCL; EL: epiligament. Original magnification: 40X

NIH-PA Author Manuscript
NIH-PA Author Manuscript
NIH-PA Author Manuscript

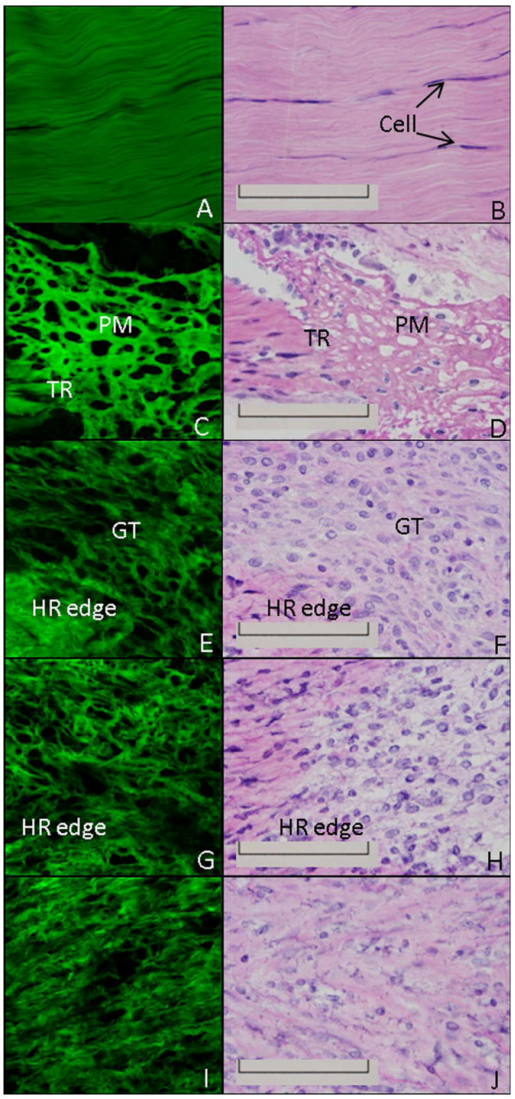

NIH-PA Author Manuscript
NIH-PA Author Manuscript
NIH-PA Author Manuscript

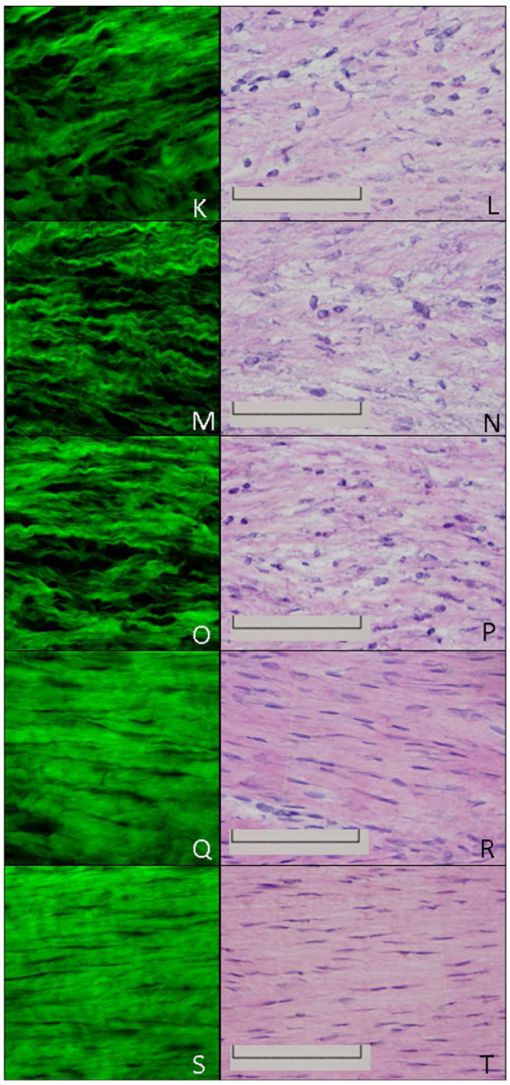

Figure 2.
H&E and MPLSM of the healing ligament. MPLSM staining (left column) and the corresponding H&E image (right column) of the normal intact (A-B) or healing ligament at 1 day (C-D), 3 days (E-F), 5 days (G-H), 7 days (I-J), 9 days (K-L), 11 days (M-N), 14 days (O-P), 21 days (Q-R) or 28days (S-T) post injury. TR: transected region; PM: provisional matrix; GT: granulation tissue; HR edge: healing region edge; Original Magnification: 600X

NIH-PA Author Manuscript

NIH-PA Author Manuscript

NIH-PA Author Manuscript

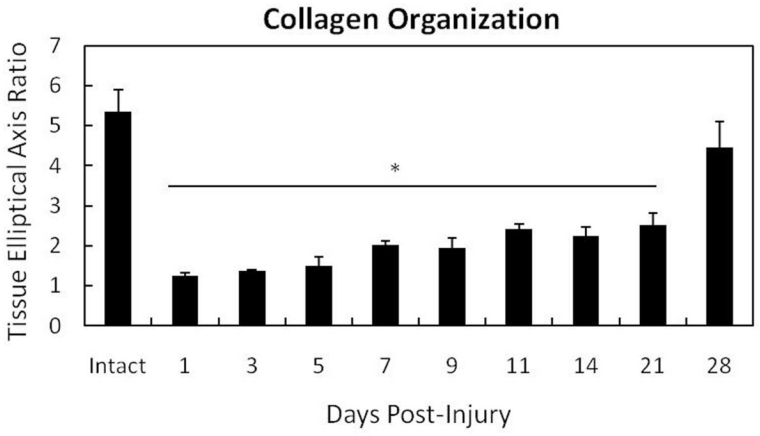

Figure 3.

Quantification of collagen disorganization using the TEAR metric (TEAR=1 represents randomly oriented fibers. Higher values show greater organization). Normal ligament (CX) exhibits greater collagen organization indicated by a higher TEAR. Injury significantly ($p < .05$) reduces collagen organization from days 1-21. Collagen orientation of the day 28 healing ligament is similar to the uninjured MCL ($p=0.056$). Asterisk indicates significance differences between the intact ligament and the day 1-21 healing ligaments. Significance was based on $p < .05$.

NIH-PA Author Manuscript
NIH-PA Author Manuscript
NIH-PA Author Manuscript

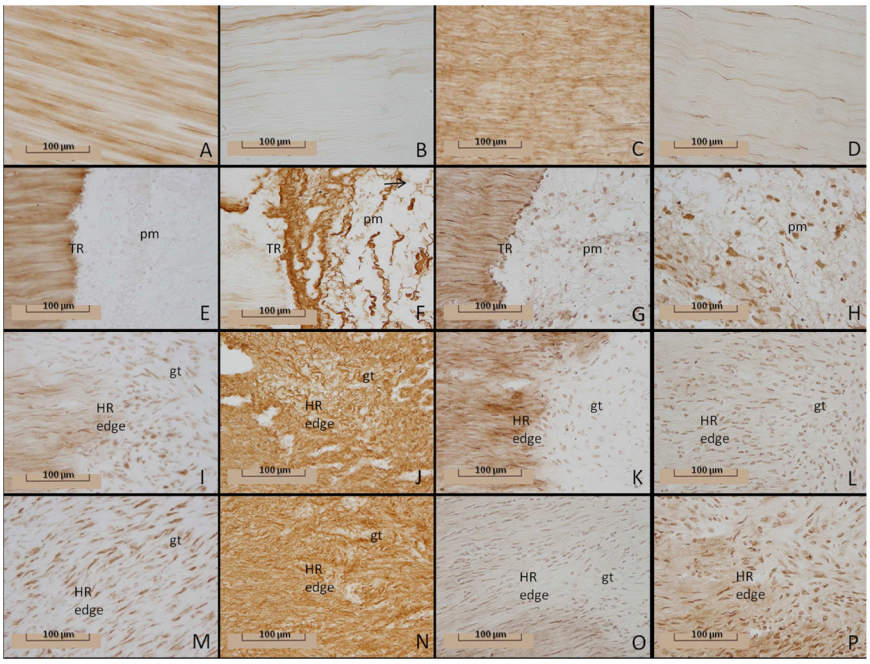

Figure 4.

Type I procollagen, type III collagen, decorin, and fibromodulin production within the healing ligament. Immunohistochemistry of type I procollagen (1 column: A, E, I, M), type III collagen (2nd column: B, F, J, N), decorin (3rd column: C, G, K, O), and fibromodulin (4th column: D, H, L, P) by the intact control or healing ligament. Images depict the normal intact (A-D) or healing ligament at 1 day (E-H), 5 days (I-L), and 7 days (M-P) post-injury. Original magnification: 400X; tr: transected region; pm: provisional matrix; gt: granulation tissue; HR edge: healing region edge (granulation tissue border).

NIH-PA Author Manuscript
NIH-PA Author Manuscript
NIH-PA Author Manuscript

A

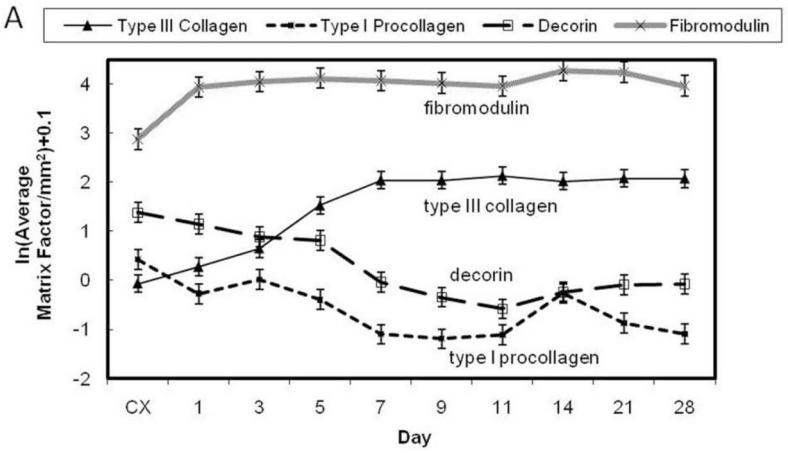

B

Day	Type I Procollagen	Type III Collagen	Decorin	Fibromodulin
CX	.428[a] (±.182)	-.066[a] (±.226)	1.378[a] (±.203)	2.875[a] (±.208)
1	-.271[a] (±.182)	.274[ab] (±.226)	1.145[ab] (±.203)	**3.938[b] (±.209)**
3	.012[ab] (±.182)	**.647[b] (±.226)**	.885[ab] (±.203)	**4.048[b] (±.209)**
5	-.398[a] (±.182)	**1.526[c] (±.226)**	**.812[b] (±.203)**	**4.119[b] (±.209)**
7	**-1.096[c] (±.176)**	**2.039[cd] (±.218)**	**-.035[c] (±.197)**	**4.068[b] (±.201)**
9	**-1.188[c] (±.177)**	**2.04[cd] (±.220)**	**-.344[cd] (±.196)**	**4.018[b] (±.203)**
11	**-1.112[c] (±.176)**	**2.13[d] (±.218)**	**-.582[d] (±.196)**	**3.959[b] (±.201)**
14	-.261[b] (±.174)	**2.02[cd] (±.215)**	**-.240[cd] (±.193)**	**4.278[b] (±.199)**
21	**-.868[c] (±.182)**	**2.078[cd] (±.226)**	**-.088[cd] (±.203)**	**4.244[b] (±.209)**
28	**-1.097[c] (±.182)**	**2.075[cd] (±.226)**	**-.073[cd] (±.203)**	**3.968[b] (±.209)**
p-value	**<.0001**	**<.0001**	**<.0001**	**<.0001**

Figure 5.

Temporal localization of the ECM factors by the healing ligament. A) Graph illustrating the temporal pattern of type I procollagen, type III collagen, fibromodulin, and decorin. B) Table demonstrating the temporal significance between days of each factor. Significance was based on $p < .05$. Within each column, significant differences are discerned by letters ([a,b,c,d]). Bold numbers indicate the most significant changes from the control values.

NIH-PA Author Manuscript
NIH-PA Author Manuscript
NIH-PA Author Manuscript

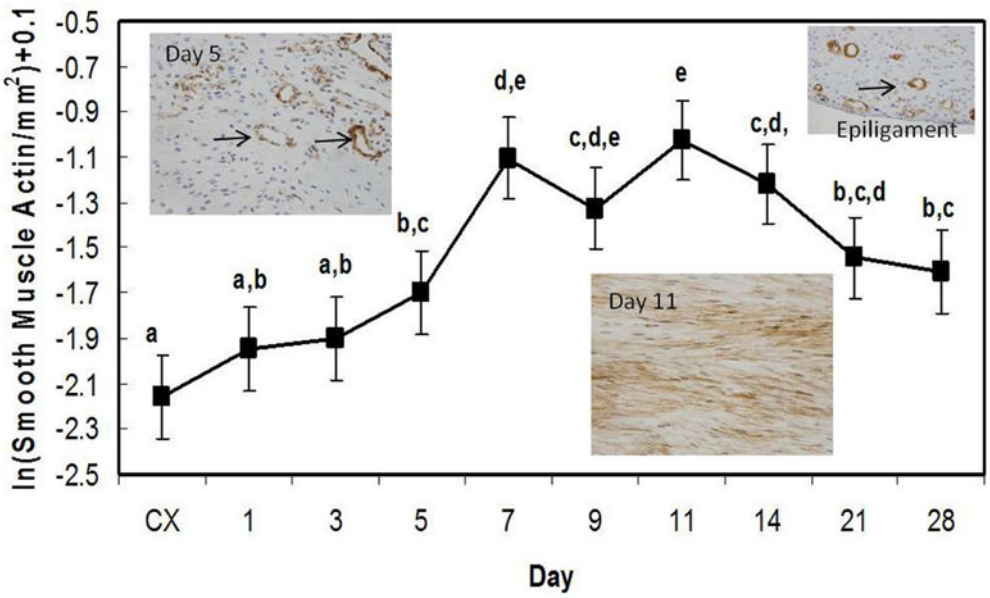

Figure 6.

Production of α-smooth muscle actin by the healing ligament. Significance was based on $p < .05$. Significant differences are discerned by letters (^{a,b,c,d,e}). Insets depict the healing ligament at day 5 (left), day 11 (middle), or epiligament (right) stained for α-SMA. Arrows indicate examples of blood vessel staining in the day 5 and epiligament insets. Myofibroblasts predominate at day 11 (middle inset).